Mechanical Properties of Nanoparticles: Characterization by In situ Nanoindentation Inside a Transmission Electron Microscope

Lucile Joly-Pottuz, Emilie Calvié, Julien Réthoré, Sylvain Meille, Claude Esnouf, Jérome Chevalier, Karine Masenelli-Varlot

Mechanical Properties of Nanoparticles: Characterization by *In situ* Nanoindentation Inside a Transmission Electron Microscope

Lucile Joly-Pottuz, Emilie Calvié, Julien Réthoré, Sylvain Meille, Claude Esnouf, Jérôme Chevalier, and Karine Masenelli-Varlot

8.1 Introduction

In situ testing inside electron microscopes has been well developed since the 1990s. Heating tests inside Environmental Scanning Electron Microscope (ESEM), tensile tests inside Scanning Electron Microscope (SEM) (dedicated to nanowires and nanotubes), heating or tensile tests inside Transmission Electron Microscope (TEM), and *in situ* nanoindentation in ESEM are increasingly performed for the observation and analysis of the thermal, environmental, or mechanical behavior of materials at the micro- or nanoscale. More than 1000 papers were published in the past 20 years, with the words "*in situ*" and "microscopy" in materials science. Nanosolicitation of materials at the nanoscale is one of the emerging methods. Andrew Minor and coauthors first published on *in situ* nanoindentation experiments inside a transmission electron microscope in 2001. This technique has since gained interest because it provides unique information on the mechanical behavior of the materials at the nanoscale or on nanoparticles. It can, indeed, be used either on thin sections of bulk materials or on nanoparticle systems. The aim of this chapter is to focus on the nanoindentation of nanoparticles. However, the introduction also presents the most important works performed on thin sections of bulk materials. Most of the *in situ* mechanical experiments performed on nanoparticles are called '*nanoindentation*'. Such tests can also be called '*nanocompression*', because they consist of a load under compression of the particles between two plateaus. We, however, continue to call these tests "nano-indentation" with reference to the previous literature in the field.

There is great interest in the characterization of mechanical properties of nanoparticles, which can reveal some key information, as far as the material performance during processing or use is considered. Nanoparticles , for example, can be used for the elaboration of materials with nanometer grain size, as reinforcement in composites materials and as additives in lubricants. The characterization of their mechanical properties and their behavior under compression is of great interest. In the case of ceramic materials, materials with nanometer grain size are

widely studied because they are expected to exhibit peculiar properties, which can be different from the properties of the materials with a bigger grain size. The elaboration of such ceramics requires the use of nanopowder. Several aspects can be optimized in the elaboration process of these nanoceramics: dispersion, grinding, green body preparation, or sintering. Knowledge of the mechanical behavior of ceramic nanoparticles during *in situ* experiments can, therefore, provide insight into their ability to deform under pressure, that is, during compaction phases (this applies to cold isostatic pressing, hot pressing, etc.), or to break/deform during grinding. One important aspect is that the structure of the material can change for nanometer-size powder, as observed in the case of alumina. Therefore, testing the particles is the only way to obtain relevant mechanical behavior laws.

8.2
In situ TEM Nanoindentation Developments

8.2.1
Description of the Sample Holder

Nanoindentation experiments inside a transmission electron microscope have been made possible through the development of specific sample holders. The limited size of the sample holder and the vacuum environment inside the microscope have led to specific requirements. Generally, such sample holders include transducers in order to move not only the sample or the tip in the three directions of space but also the sensors to measure the operating forces. An example of the experimental setup is presented in Figure 8.1.

Since 1997 and the first publication on *in situ* nanoindentation [1, 2], several groups have developed homemade sample holders [3, 4] that are compatible with their own microscopes (Table 8.1). Commercial sample holders are now available on the market. Two types of sample holders can be distinguished, depending on the moving part (sample or tip). Moreover, single-tilt or double-tilt sample holders are available. The latter can be very useful to perform experiments on crystalline

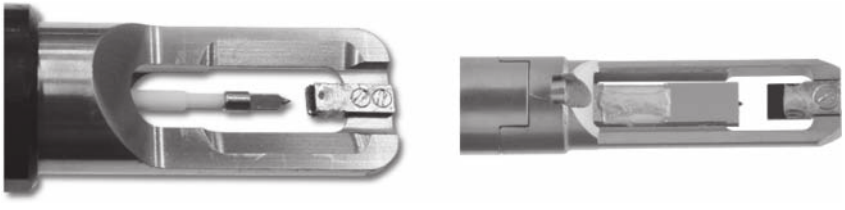

(a) (b)

Figure 8.1 Examples of *in situ* TEM nanoindentation sample holder front end designed for (a) JEOL and (b) FEI microscopes. In these two configurations, the sample is fixed and the movement is ensured by the tip. Courtesy of Hysitron, Inc.

Table 8.1 Development of nanoindentation sample holder.

Year	Authors	Development	References
1997	Wall, M.A., Dahmen U	Sample holder for a 1.5 MeV electron microscope	[1]
1998	Wall, M.A., Dahmen U	Sample holder for a JEOL 200CX	[2]
2001	Stach, E.A. *et al.*	Particular interest on the sample geometry	[3]
2005	Bobji, M.S. *et al.*	Sample holder for a JEOL 2010	[4]

materials on a specific zone axis. The most important requirement is accurate positioning of the moving part. The use of piezoelectric materials leads to sub-angstrom resolution in the x, y, and z positions. Nevertheless, aligning the tip and the sample is not a trivial task because of the microscope depth of field. First, the part that remains fixed is placed at the reference height, which usually is the eucentric position. Further, the Z positioning of the moving part is performed by using an image wobbler. Bragg fringes can be used to determine whether the moving part is above or below the stationary part.

Several tip geometries, including Berkovich and Vickers tips and truncated cones or wedges, can be considered depending on the type of samples studied. Wedges are well adopted for experiments on thin sections because they can avoid sample sliding under compression. The punch tip can rather be used for nanoparticles because its large flat area large allows for the control of the sample geometry in the nanoindentation experiment; thus, a pure compression test can be performed. The use of a tip with a specific radius of curvature can lead to modeling of a more complex system. However, it is difficult to provide more precise recommendation, because the choice of the tip strongly depends on the sample nature and geometry.

8.2.2 Sample Geometry

Three main sample geometries can be envisaged for TEM *in situ* nanoindentation experiments: nanopillars, thin sections, and nanoparticles. Nanopillars and nanoparticles are geometries dedicated to the characterization of nanoscale mechanical properties of materials, while thin sections are rather used to study the grain evolution and interphase or dislocation movement. In the case of nanopillars and thin sections, the samples need to be milled from bulk materials. Focused ion beam (FIB) is obviously the key technique used for such sample preparation. However, depending on the technique used, defects and deformation or amorphization of the sample can be induced. This aspect needs to be taken into account for the experiment and data processing interpretation. Table 8.2 summarizes several studies using several geometries.

Table 8.2 Studies performed on different sample geometries using a nanoindentation sample holder.

Sample geometry	Materials	References	Comments
Nanopillars	Silicon	[5]	SEM nanoindentation experiments
Nanopillars	Vanadium	[6]	
Nanopillars	Molybdenum crystal	[7]	TEM experiments
Nanopillars	Mg and Mg–Ce	[12]	
Nanopillars	Metal glasses	[8]	
Thin sections	Iron–3% silicon crystal	[14]	
Thin sections	Metal	[15]	
Thin sections	Alumina–zirconia–magnesia	[16]	
Thin sections	Zirconia	[9, 10, 14–20]	
Silicon wedge substrate	Aluminum	[10]	
Silicon wedge substrate	Al–Mg	[17]	
Clusters of nanoparticles	Si	[11]	
Isolated nanoparticles	Alumina with 100 nm diameter	[27–29]	
Isolated nanoparticles	Silicon with 200–250 nm diameter	[22, 23]	
Isolated nanoparticles	Silica	[25]	
Isolated nanoparticles	CdS with 200–400 nm	[26]	

As far as nanopillars are concerned, they have been used for *in situ* nanoindentation experiments not only in TEM but also in SEM or Atomic Force Microscope (AFM). In SEM, for example, the brittle–ductile transition and the size effect in silicon [5] and vanadium [6] have been investigated. Deformation mechanisms and plasticity effects, such as the evolution of a defect-free molybdenum crystal, have been considered in TEM [7] (see Figure 8.2a for a typical configuration). In order to avoid any defects being induced by FIB milling, *in situ* TEM annealing was preliminary performed. Deformation mechanisms by basal plane sliding or extension twinning were found to be size dependent in the case of Mg and Mg–Ce crystals [12]. The ability of metallic glasses to sustain large plastic strains can also be considered during *in situ* compression of nanopillars [8].

Thin sections are well-known samples for TEM observations. One of the major drawbacks of thin sections is their propensity to be bent during the *in situ* nanoindentation experiment, which complicates the strain tensor and then renders the interpretation of the observed contrast more difficult. One way to hinder this undesired phenomenon is to use a "H-bar" geometry, which is composed of a thick section with only a small electron-transparent region close to the edge and is schematically represented in Figure 8.2b [9, 13]. One of the main applications of the experiments on thin sections is, for example, the study

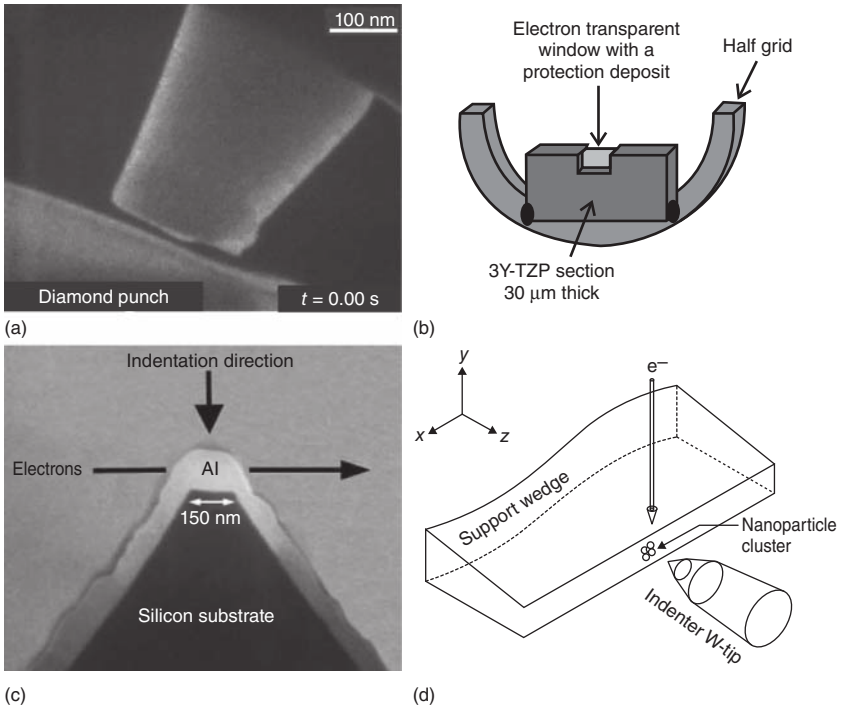

Figure 8.2 Different sample geometries for *in situ* TEM nanoindentation experiments. (a) nanopillar [8], Reprinted figure with permission from [8]. Copyright (2013) by the American Physical Society; (b) thin foil [9]; (c) thin film [10], with permission from Elsevier; and (d) nanoparticles or clusters [11], with permission from the American Institute of Physics.

of dislocation movements and grain boundary activities in metals [14, 15] or in ceramics [16]. To avoid the artifacts that can be induced by ion milling, thin coatings can alternatively be deposited on a wedge-shaped silicon substrate [10, 17] (see Figure 8.2c). The *in situ* experiment interpretation is not an easy task because the contrasts in the images need to be analyzed. Simulations can be carried out to calculate the stress distribution on the entire thin section during the indentation process [18]. Stresses can also be experimentally determined from the convergent beam electron diffraction (CBED) patterns [19]. This technique has recently been used to highlight the nanodomains that can act as embryos during the phase transformation in zirconia [20].

One of the main advantages of the geometry of nanoparticles (see Figure 8.2d) lies in their ability to easily model a nanoindentation system. Indeed, the movement of the two homologues (substrate and tip) of the nanocompression system can be monitored during the experiment, provided that they are perpendicular to the electron beam. The second advantage is that preparation of the sample (cutting and thinning) is not required before the experiment. Nevertheless, dispersion of the nanoparticles in a solvent can lead to certain surface modification.

In contrast to nanopillars and thin sections prepared from bulk materials, nanoparticles need to be deposited on a substrate. The choice of the substrate, in that case, is crucial. Its geometry needs to be optimized, and specific attention needs to be paid to its thickness. In the case of a very thin sample, the nanoparticles can easily slide along the substrate during the nanoindentation. In the case of a very thick substrate, certain shadowing effect can occur (see Figure 8.3). It can lead to certain problems during data processing, for example, determination of the contact area between the particle and the substrate. Figure 8.4 shows an example of such system, where the positions of the tip and the substrate

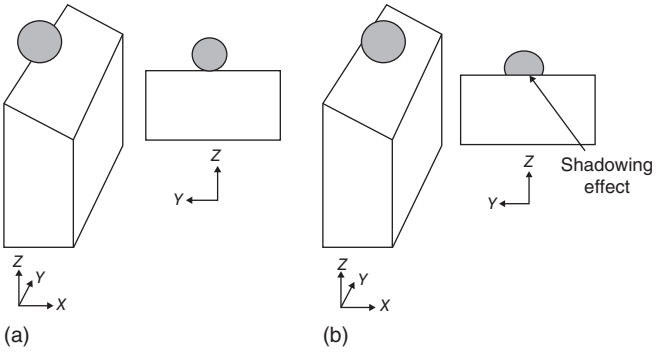

Figure 8.3 Schematic representation of the shadowing effect in the case of a thick substrate (electron beam along the *x* direction and nanoindentation along the *z* axis); (a) the nanoparticle is well positioned, (b) the nanoparticle slides on the substrate and is not fully observed in the *x* direction.

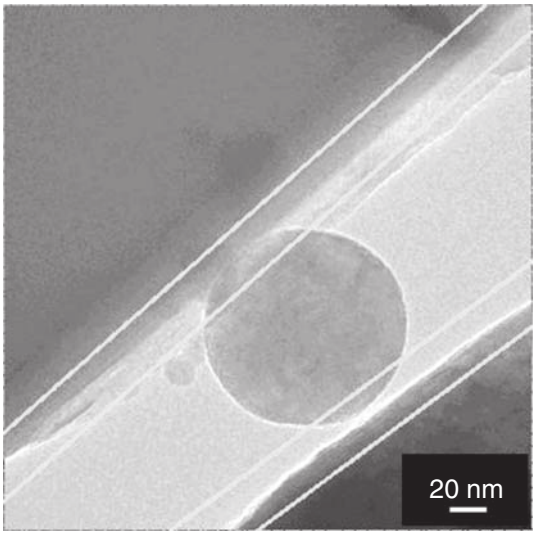

Figure 8.4 Example of a nanoparticle system and determination of the position of the tip and the substrate.

can be accurately determined in addition to the particle contour. The nature of the substrate is also a key parameter. Its hardness should be higher than that of the nanoparticles under study; otherwise, the substrate can deform during compression. Finally, its surface needs to be as smooth as possible in order to achieve good distribution of the force applied on the nanoparticle. Finally, it can be mentioned that contamination of the tip can occur and is very difficult to be removed. For small-diameter nanoparticles, this contamination layer can also hinder good observation of the contact between the tip and the nanoparticle.

The analysis of a single particle requires an initial very good dispersion of the nanoparticles on the substrate. It is necessary to remove some of the particles by slightly rubbing the surface of the substrate with the tip. Dispersion of the nanoparticles in a solvent before deposition should be performed, if possible, without the use of a dispersant. The dispersant can, indeed, remain on the surface of the nanoparticles and, consequently, modify the nanoindentation experiments. The nanoparticles can also be affixed to a metal wire by dry dripping [21].

The behavior of single nanoparticles can be easily modeled in terms of the mechanical system; however, it is difficult to perform experiments on them. The nanoparticles can, indeed, slide or be ejected from the substrate during the experiments. This difficulty increases with the decrease in their size. The diameter of the nanoparticles generally studied is about 200 nm and can be as large as 500 nm. Experiments on nanoparticles with diameters below 100 nm require a very precise tip/nanoparticle/substrate alignment. Good orientation of the nanoparticles toward the electron beam is also a very difficult task. It is rather difficult to orientate a nanoparticle in the TEM, and the best way is to determine a nanoparticle that is already well oriented. Furthermore, the nanoparticles can easily be removed during the adjustment of the alignment due to vibrations or irradiation of the electron beam.

8.3
Examples of *In situ* Nanoindentation Tests on Nanoparticles

8.3.1
Clusters

A few experiments have been reported so far on the characterization of clusters. One study was on Si nanoparticle clusters [11]. It demonstrated the rotation of the nanoparticles inside the cluster to relieve the stress during deformation. Further, a fracture was observed at the junction between two Si nanoparticles, within the amorphous Si layer. The propagation of the crack along the interface permits the cluster to deform and relieve the applied strain, with each remaining fragment deforming elastically to regain its initial morphology.

8.3.2
Isolated Nanoparticles

Isolated nanoparticles are widely studied by *in situ* nanoindentation to observe their behavior in real time and to determine their mechanical behavior. First, experiments were performed on silicon nanoparticles with a diameter of 200–250 nm [22, 23]. Both elastic and plastic deformations were observed, followed by a fracture. The fracture load was determined by scanning probe microscopy (SPM) [24]. Nevertheless, the major advantage of transmission electron microscopy is the possibility to observe the fracture in real time to determine the mechanisms that trigger it. Furthermore, it is possible to correlate the evolution of the microstructure and the load–displacement curves.

The nanoparticles generally studied have a quite large diameter, for example, 500 nm for amorphous silica nanoparticles [25] or 200 to 400 nm for CdS hollow spheres [26]. Smaller nanoparticles of 100 nm were recently studied [27]. The transition alumina tested was plastically deformed during nanocompression. This result is of great interest for the optimization of the compaction process before sintering. This alumina is, indeed, used to obtain alumina bulk material with nanometer-size grains.

Independently of their nature, the aforementioned studies indicate that large nanoparticles break during the *in situ* experiment while the smallest ones undergo large plastic deformation. An analysis of the nanoparticle behaviors as a function of their diameters can be of interest to investigate a possible nano effect and the corresponding critical nanoparticle size. It seems that the plastic behavior can, indeed, be size dependent because, in the same transition alumina nanoparticles with a diameter above 100 nm, failure was observed – either before or after plastic deformation. This discrepancy in the behavior of ceramic nanoparticles can explain the grinding limit observed for ceramic nanopowder.

8.4
Data Processing

Two major results are obtained from an *in situ* nanoindentation experiment:

- Images or movies
- Load–displacement curves.

The entire data process involves interpretations of both the contrast of the images and the interpretation of the curves. Nevertheless, the most important aspect is the relationship between the phenomena observed on the images and on the curves.

8.4.1
Contrast Imaging

The contrast observed for nanoparticles during the experiments is difficult to interpret. Indeed, the changes in the contrast can be due to the thickness changes, bending of the sample, stress contours, or presence of dislocations. Nevertheless, nanoindentation experiments on nanoparticles present several specificities, and the contrast origin needs to be discussed further. Carlton *et al.* [21] well described the problems and advantages of either diffraction contrast or phase contrast during *in situ* TEM nanoindentation. In the case of diffraction contrast, the alignment of the nanoparticle along a particular beam direction is not obvious and becomes very difficult for small nanoparticles, because small vibrations during tilting of the substrate can lead to their removal. Bending of the sample does not seem to be possible in the case of a nanoparticle, because nanoparticles can roll or slide along the support or be removed before bending. Deneen *et al.* [22] described the bands of contrast in Si nanoparticles at the points of contact between both the substrate and the tip. These bands are due to the local bending of the lattice planes. They disappear when the tip is removed, which proves the elastic type of the deformation. An increased diffraction contrast at the top and bottom of the spheres was attributed to plastic deformation [28]. Interpretation of the contrast is not obvious and can be completed either by other imaging techniques or by simulations tools (see Section 8.4).

Among the other imaging techniques, dark field imaging can be considered. It was used to monitor the grain size evolution during the compression test or certain changes in the nanoparticles. In the case of hollow CdS spheres, there were no changes in the grain size observed in the nanoparticles before and after the compression tests [26]. The area of plastic deformation was observed on silicon nanospheres [22] after sufficient deformation. The use of an analytical tool such as electron energy loss spectroscopy (EELS) can be envisaged. This technique can be very useful to determine the structural changes in the nanoparticles during the experiment. It has been, for example, used to monitor eventual crystallization of amorphous silica during compression [25]. In the case of transition alumina, EELS can allow for eventual phase transformation during the nanoindentation experiments.

8.4.2
Load–Displacement Curve Processing

For a quantitative study with the calculation of forces and stresses applied on nanoparticles, the main problems are the evaluation of the real contact area between the tip and the nanoparticles and accurate determination of the 3D geometries of both the tip and the sample. The data processing, thus, requires specific attention in order to obtain accurate values.

The use of an image registration technique is crucial in order to obtain robust and accurate estimates of the motion of the specimen holder and the tip. Indeed,

as it is the case for most of the testing devices at the meter scale, the specimen holder cannot be considered as infinitely stiff as compared to the tested particle. Thus, during mechanical testing of the holder and the tip experience motion, as the displacement motion is evaluated by the piezoelectric actuator that is far from the contact area between the holder and the particle, the displacement measurement from the actuator is inaccurate for a quantitative description of the load–displacement curves. To circumvent this difficulty, the images acquired during the test are analyzed using an image registration technique. The motion of the area delimited by the yellow lines in Figure 8.4, in the direction normal to the contact planes, is evaluated. For each solid (specimen holder and tip), only a global translation normal to the contact plane is considered; thus, the algorithm reveals extreme robustness. From the image registration, the relative displacement (in pixel) between the specimen holder and the tip is converted into nanometer using the scale bar of the images. The actual solicitation applied to the nanospecimen is thus evaluated; see Figure 8.5 for a comparison with the data provided by the piezoelectric actuator. This relative displacement is then used in the finite element (FE) simulation (see Section 8.4) as the boundary conditions and the response of the model in terms of the load–displacement curve are compared to the experiments.

8.4.3
Effect of the Electron Beam

One important aspect regarding the determination of the mechanical properties of the materials at the nanoscale by *in situ* TEM nanoindentation is probably the effect of the electron beam. The irradiation effect can, indeed, occur and modify not only the chemical and/or crystallographic structure of the material but also its mechanical behavior. This phenomenon was evidenced by Zheng *et al.* [25] during *in situ* compression of silica nanoparticles with 100 nm diameter. Plastic deformation of the nanoparticles was observed, and a much easier plastic flow

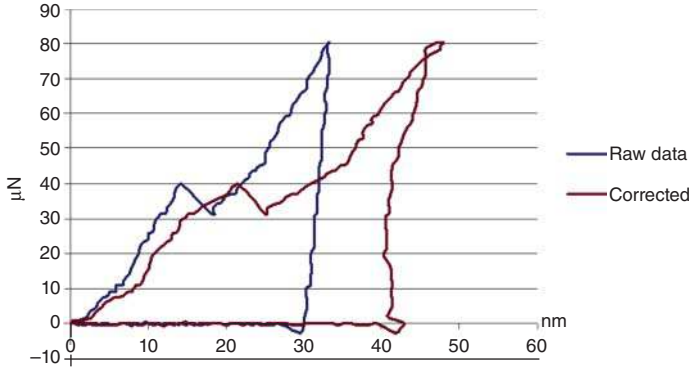

Figure 8.5 Comparison of the load–displacement curves before and after correction.

was observed when the electron beam was on compared to the experiment when the beam was off as shown in (Figure 8.6).

As far as crystalline materials are concerned, a plastic behavior has been observed in alumina nanoparticles during *in situ* TEM compression (Figure 8.6a,b). The observation of a thin section obtained from alumina compressed at room temperature in a high-pressure cell confirms the plastic deformation of nanoparticles (Figure 8.7). These results prove that the plastic behavior can occur even without the effect of electron beam on materials that are known to exhibit a brittle behavior at the macroscopic scale [29]. From these two studies, we can assume that the electron beam have an effect on the values obtained for the mechanical properties; however, the mechanical behavior (plastic behavior) cannot be attributed only to the effect of the electron beam.

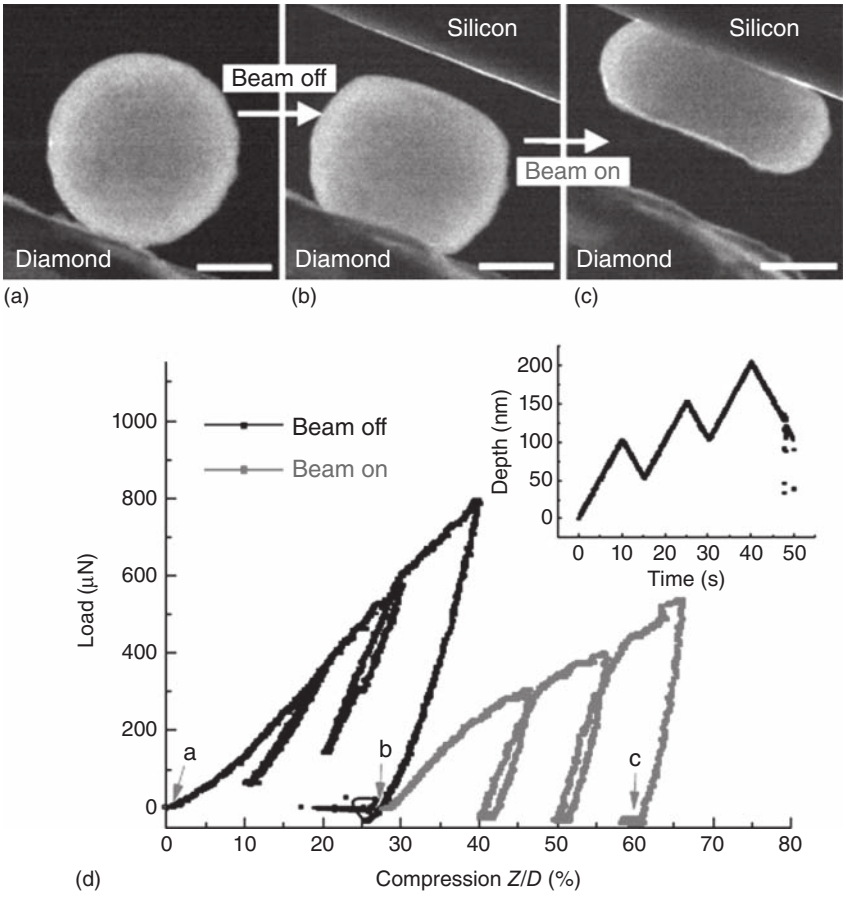

Figure 8.6 TEM dark field images of silica nanoparticles [25]: (a) before nanocompression and after compression (b) without electron beam, (c) with electron beam; (d) corresponding load–compression curve (points a, b, and c correspond to the images). With permission from Nature Publishing group.

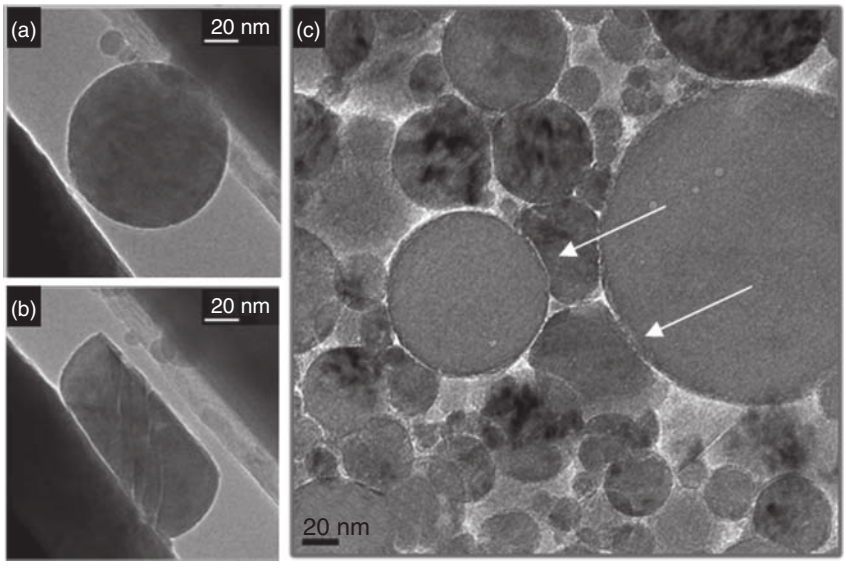

Figure 8.7 TEM images of transition alumina nanoparticles (a) before; (b) during nanocompression experiment; (c) TEM image of a thin section obtained from the same alumina powder compacted at ambient temperature under a pressure of 5 GPa.

8.5
Interest of Simulation on the Data Processing

Analysis of the load–displacement curves once processed can be first performed using certain analytical models. The well-known Hertz model for the elastic contact between two surfaces is used in nanoindentation with spherical tips. It can be applied to the case where a compression load is applied to a spherical nanoparticle in order to determine the reduced modulus, by combining the elastic properties of the particles and the compression platens. Once the properties of the loading platens are known, the Young's modulus of the particle can be estimated.

Numerical simulation can be used to complete and interpret the results obtained during *in situ* testing.

Models can be developed to explain either the fracture or the plasticity of the nanoparticles. In the case of CdS nanoparticles (Figure 8.8), the fracture occurs perpendicular to the compression planes as encountered in the case of Brazilian test [26]. This test is well known in the case of characterizing the tensile strength of ceramic materials. In the case of these hollow nanoparticles, the model used can be different. To understand the fracture mode, it is necessary to assess the stress state within the spheres during deformation and at the point of fracture. FE simulations were used along with a pure elastic behavior.

Zheng *et al.* [25] also used FE simulations in the case of amorphous silica nanoparticles, along with a purely elastic model. The model used is, in fact, of much importance and is well defined. Shan used FE analyses to determine the

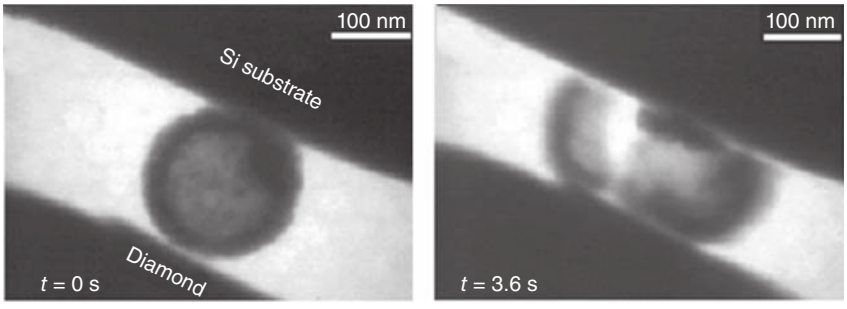

(a) (b)

Figure 8.8 Compression experiments on a hollow CdS nanosphere: (a) initial state and (b) after failure [26] With permission from Nature Publishing group.

stress state within the spheres during deformation and at the point of fracture, with a purely elastic model.

To explain the plasticity of nanoparticles, the models describing the movement of dislocation are the most appropriate. Gerberich *et al.* [30] developed a model describing the dislocation movement in a cylinder (Figure 8.9). During the loading–unloading experiment, the dislocations movement inside the cylinder can be induced or annihilated. After several cycles, it is noticed that the plasticity is mainly due to the movement of the existing dislocations, as described on Figure 8.5b.

FE simulations can be used to determine the constitutive law for nanosolicitation tests. Calvie *et al.* [29] proposed a method by which the constitutive law is

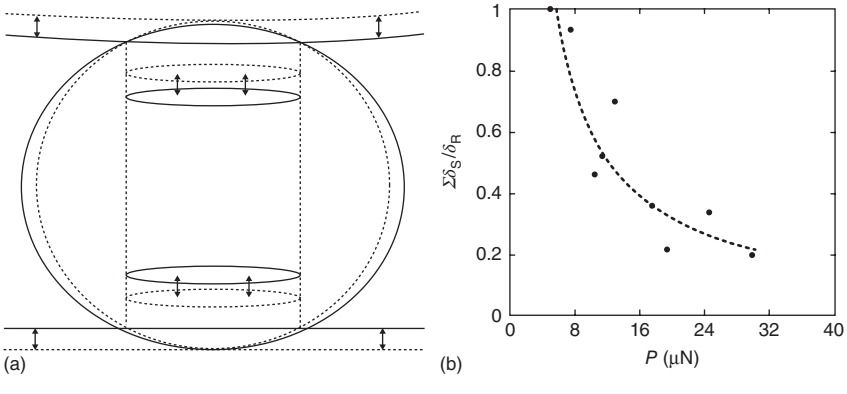

(a) (b)

Figure 8.9 (a) Model of the compression of a nanoparticle. The plasticity of the nanoparticle can be explained by the movement of the dislocation inside the cylinder; (b) fraction of plasticity for dislocations nucleated or annihilated. It indicates that, after several cycles, the residual plasticity is associated with the moving pre-existing dislocations [30]. With permission from Elsevier.

Table 8.3 Young's modulus and yield stress obtained from the data processing by FE and analytical method on alumina nanoparticles.

Finite element simulation loading curve		Analytical method		
		Loading curve		Unloading curve
E (GPa)	σ_y (GPa)	E (GPa)	σ_y (GPa)	E (GPa)
115	10	113	8	113

determined by fitting of the loading–unloading curves obtained during the experiment. The results obtained by FE are confirmed by an analytical method based on fitting of the elastic part of the loading curve with a Hertzian model and fitting of the unloading curve by a power-law function through the classical Oliver–Pharr model (Table 8.3). Both the methods allow for the determination of the elastic modulus; furthermore, the elastic limit has also been estimated analytically as the mean pressure at the end of the elastic domain of the loading curve. The main aspect of the experiment performed on the transition alumina is that it is only stable at the nanometer scale. The bulk material of this alumina, thus, does not exist. The values obtained for Young's modulus can be compared with another nanometer-size stable alumina phase: γ-alumina compacted under high pressure. A value of 253 GPa was obtained, which is twice the value obtained during *in situ* nanoindentation in TEM [31]. This discrepancy can be explained by the effect of the electron beam, as measured by Zheng *et al.* [25]. However, other parameters such as particle orientation, the different features of the starting powder, and difficulties in obtaining Young's modulus of the powder compacts from high-pressure vessel experiments limit the possibility to compare the two types of values obtained.

Furthermore, it is possible to calculate the map of the total equivalent plastic strain of the nanoparticle using the determined constitutive law. In the case of alumina particles, the calculated map perfectly matches with the contrast observed on the TEM image (Figure 8.10). The observed Bragg fringes can be attributed to plastic deformation and not to elastic lattice compression, as it has already been theoretically calculated [21].

Simulation by FE can also be used to determine a Tresca shear–strain map (Figure 8.11). Good correlation can be observed between the map and the cracks in an alumina nanoparticle. It also indicates that the crack occurs by shearing.

Molecular dynamics (MDs) simulations can provide valuable pieces of information regarding the deformation mechanisms at the nanoscale. They are used to better understand the response of amorphous silica theoretically [32, 33] or to better analyze the results obtained during *in situ* testing and the effect of the electron beam on the results [25]. In the case of crystalline materials, the formation and movement of dislocations are studied [34–36].

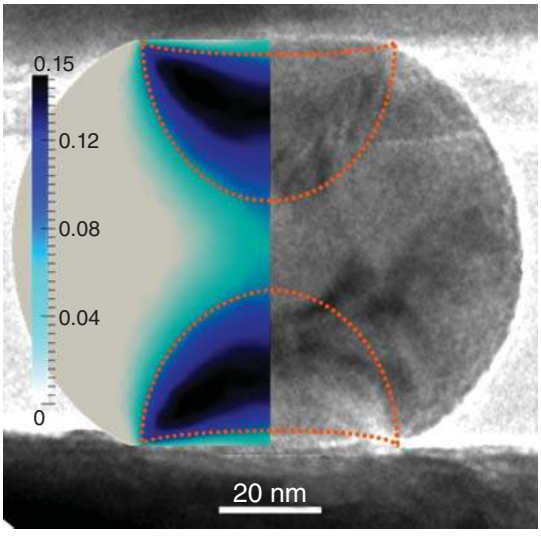

Figure 8.10 Superposition of an experimental image with the corresponding map of the total equivalent plastic strain calculated by DIC-FE. A good agreement between the experimental image and the calculated map is observed. (The contours of the maximum equivalent plastic strain are highlighted with dotted lines.) It indicates that the observed Bragg fringes are caused by plastic deformation.

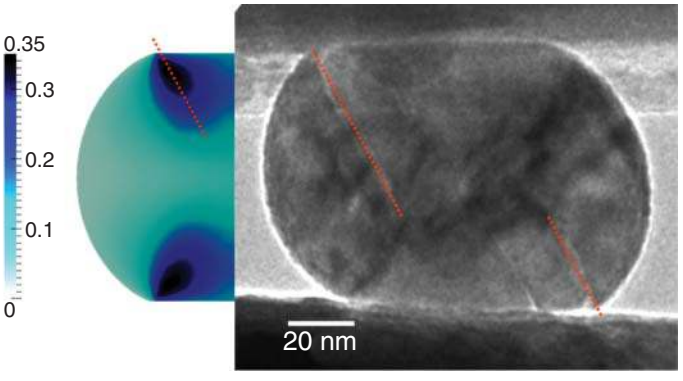

Figure 8.11 Superposition of an experimental image with the corresponding map of the Tresca shear–strain calculated by FE in the case of an alumina nanoparticle. A good agreement between the experimental image and the calculated map indicates that the crack occurs by shearing (the crack is indicated by a dashed line).

8.6 Conclusion

In this chapter, we emphasized on *in situ* nanoindentation of particles inside a TEM. A methodology to test isolated particles and to obtain relevant load–displacement curves in order to capture the real nanoparticle behavior

needs to be developed to fully interpret the results obtained. Simulation tools are widely used to complete the imaging and obtain the load–displacement curves results. By a careful follow-up of the load versus real displacement curves, the mechanical behavior law of a given nanoparticle can be obtained. It is demonstrated, for example, that the elastic–plastic behavior of ceramic nanoparticles that behave as truly brittle at the macroscale can be recorded, with access to not only their Young's modulus but also their elastic limit and plastic behavior law. By *in situ* experiments of this type, plastic deformation of powder compacts can be conducted at room or moderate temperature, which opens the door to new strategies for the processing of materials, for example, compaction of ceramics before sintering. The critical size above which the particles can fail and below which the particles are deformed plastically without failure even after large deformation can be determined. This critical size can explain the grinding limit often reported in ceramic science.

The example provided on the aforementioned ceramic particles showed that *in situ* TEM testing provides new insights on the mechanical behavior of the materials at the nanoscale, with impacts their process and their use.

References

1. Wall, M.A. and Dahmen, U. (1997) Development on an in situ nanoindentation specimen holder for the high voltage electron microscope. *Microsc. Microanal.*, **3**, 593–594.
2. Wall, M.A. and Dahmen, U. (1998) An in situ nanoindentation specimen holder for a high voltage transmission electron microscope. *Microsc. Res. Tech.*, **42**, 248–254.
3. Stach, E.A., Freeman, T., Minor, A.M., Owen, D.K., Cumings, J., Wall, M.A., Chraska, T., Hull, R., Morris, J.W., Zettl, A. Jr., and Dahmen, U. (2001) Development of a nanoindenter for in situ transmission electron microscopy. *Microsc. Microanal.*, **7** (06), 507–517.
4. Bobji, M.S., Pethica, J.B., and Inkson, B.J. (2005) Indentation mechanics of Cu–Be quantified by an in situ transmission electron microscopy mechanical probe. *J. Mater. Res.*, **20**, 2726–2732.
5. Ostlund, F., Rzepiejewska-Malyska, K., Leifer, K., Hale, L.M., Tang, Y., Ballarini, R., Gerberich, W.W., and Michler, J. (2009) Brittle-to-ductile transition in uniaxial compression of silicon pillars at room temperature. *Adv. Funct. Mater.*, **19**, 2439–2444.
6. Han, S.M., Bozorg-Grayeli, T., Groves, J.R., and Dix, W.D. (2010) Size effects on strength and plasticity of vanadium nanopillars. *Scr. Mater.*, **63**, 1153–1156.
7. Lowry, M.B., Kiener, D., LeBlanc, M.M., Chisholm, C., Florando, J.N., Morris, J.W. Jr., and Minor, A.M. (2010) Achieving the ideal strength in annealed molybdenum nanopillars. *Acta Mater.*, **58**, 5160–5167.
8. Shan, Z.W., Li, J., Cheng, Y.Q., Minor, A.M., Syed Asif, S.A., Warren, O.L., and Ma, E. (2008) Plastic flow and failure resistance of metallic glass : insight from in situ compression of nanopillars. *Phys. Rev. B*, **77**, 155419.
9. Calvié, E., Joly-Pottuz, L., Esnouf, C., Douillard, T., Gremillard, L., Malchère, A., and Masenelli-Varlot, K. (2013) A global investigation into in situ nanoindentation experiments on zirconia: from the sample geometry optimization to the stress nanolocalization using convergent beam electron diffraction. *J. Microsc.*, **249**, 99–110.
10. Jin, M., Minor, A.M., Stach, E.A., and Morris, J.W. Jr., (2004) Direct observation of deformation-induced grain growth during the nanoindentation of

ultrafine-grained Al at room temperature. *Acta Mater.*, **52**, 5381–5387.
11. Lockwood, A. and Inkson, B. (2009) In situ TEM nanoindentation and deformation of Si nanoparticle clusters. *J. Phys. D Appl. Phys.*, **42**, 035410.
12. Ye, J., Mishra, R.K., Sachdev, A.K., and Minor, A.M. (2011) In situ TEM compression testing of Mg and Mg-0.2 wt.% Ce single crystals. *Scr. Mater.*, **64**, 292–295.
13. Li, J., Malis, T., and Dionne, S. (2006) Recent advances in FIB-TEM specimen preparation techniques. *Mater Charact*, **57** (1), 64–70.
14. Zhang, L., Ohmura, T., Seikido, K., Nakajima, K., Hara, T., and Tsuzaki, K. (2011) Direct observation of plastic deformation in iron-3% silicon single crystal by in situ nanoindentation in transmission electron microscopy. *Scr. Mater.*, **64**, 919–922.
15. De Hosson, J.T.M., Soer, W.A., Minor, A.M., Shan, Z., Stach, E.A., Syed Asif, S.A., and Warren, O.L. (2006) In situ TEM nanoindentation and dislocation-grain boundary interactions: a tribute to Dabid Brandon. *J. Mater. Sci.*, **41**, 7704–7719.
16. Lee, J.H., Kim, I., Hulbert, D.M., Jiang, D., Mukherjee, A.K., Zhang, X., and Wang, H. (2010) Grain and grain boundary activities observed in alumina-zirconia-magnesia spinel nanocomposites by in situ nanoindentation using transmission electron microscopy. *Acta Mater.*, **58**, 4891–4899.
17. Soer, W.A., De Hosson, J.T.M., Minor, A.M., Morris, J.W. Jr., and Stach, E.A. (2004) Effects of solute Mg on grain boundary and dislocation dynamics during nanoindentation of Al-Mg thin films. *Acta Mater.*, **52**, 5783–5790.
18. De Knoop, L., Reboh, S., and Legros M. (2012) In situ TEM-nanoindentation of a silica-aluminum bilayer. Proceedings of the Electron Microscopy Congress, Manchester, UK, September 16-21, 2012, *http://emc2012.org.uk/proceedings/* (accessed 11 July 2013).
19. Banhart, F. (1994) Strains in crystals with amorphous surface films studied by convergent beam electron diffraction and high-resolution imaging. *Ultramicroscopy*, **56**, 233–240.
20. Calvié, E., Joly-Pottuz, L., Esnouf, C., Douillard, T., Gremillard, L., Malchere, A., Chevalier, J., and Masenelli-Varlot, K. (2013) Evidence for the formation of distorted nanodomains involved in the phase transformation of stabilized zirconia by coupling convergent beam electron diffraction and in situ TEM nanoindentation. *Acta Mater.*, **61**, 174–182.
21. Carlton, C.E. and Ferreira, P.J. (2012) In situ TEM nanoindentation of nanoparticles. *Micron*, **43**, 1134–1139.
22. Deneen, J., Mook, W.M., Minor, A.M., Gerberich, W.W., and Barry Carter, C. (2006) In situ deformation of silicon nanospheres. *J. Mater. Sci.*, **41**, 4477–4483.
23. Nowak, J.D., Mook, W.M., Minor, A.M., Gerberich, W.W., and Barry Carter, C. (2007) Fracturing a nanoparticle. *Philos. Mag.*, **87**, 29–37.
24. Mook, W.M., Nowak, J.D., Carter, C.B., Mukherjee, R., Girshick, S.L., McMurry, P.H., and Gerberich, W.W. (2007) Compressive stress effects on nanoparticle modulus and fracture. *Phys. Rev. B*, **75**, 214112.
25. Zheng, K., Wang, C., Cheng, Y.Q., Yue, Y., Han, X., Zhang, Z., Shan, Z., Mao, S.X., Ye, M., Yin, Y., and Ma, E. (2010) Electron-beam-assisted superplastic shaping of nanoscale amorphous silica. *Nat. Commun.*, **1**, 1–24.
26. Shan, Z.W., Adesso, G., Cabot, A., Sherburne, M.P., Syed Asif, S.A., Warren, O.L., Chrzan, D.C., Minor, A.M., and Alivisatos, A.P. (2008) Ultrahigh stress and strain in hierarchically structured hollow nanoparticles. *Nat. Mater.*, **7**, 947–952.
27. Calvié, E., Joly-Pottuz, L., Esnouf, C., Clément, P., Garnier, V., Chevalier, J., Jorand, Y., Malchere, A., Epicier, T., and Masenelli-Varlot, K. (2012) Real time TEM observation of alumina ceramic nano-particles during compression. *J. Eur. Ceram. Soc.*, **32**, 2067–2071.
28. Nowak, J.D., Beaber, A.R., Ugurlu, O., Girshick, S.L., and Gerberich, W.W. (2010) Small size strength dependence

on dislocation nucleation. *Scr. Mater.*, **62**, 819–822.

29. Calvié, E., Réthoré, J., Joly-Pottuz, L., Meille, S., Chevalier, J., Garnier, V., Jorand, Y., Esnouf, C., Epicier, T., Quirk, J.B. (2014) Masenelli-Varlot K., Mechanical behavior law of ceramic nanoparticles from transmission electron microscopy in situ nano-compression tests, *Materials Letters*, **119**, 107–110.
30. Gerberich, W.W., Mook, W.M., Cordill, M.J., Carter, C.B., Perrey, C.R., Heberlein, J.V., and Girshick, S.L. (2005) Reverse plasticity in single crystal silicon nanospheres. *Int. J. Plast.*, **21**, 2391–2405.
31. Gallas, M.R. and Piermarini, G.J. (1994) Bulk modulus and Young's modulus of nanocrystalline γ-alumina. *J. Eur. Ceram. Soc.*, **77**, 2917–2920.
32. Léonforte, F., Tanguy, A., Wittmer, J.P., and Barrat, J.L. (2006) Inhomogeneous elastic response of silica glass. *Phys. Rev. Lett.*, **97**, 055501.
33. Tanguy, A., Leonforte, F., and Barrat, J.L. (2006) Plastic response of a 2D Lennard-Jones amorphous solid: detailed analysis of the local rearrangements at very slow strain rate. *Eur. Phys. J. E*, **20**, 355–364.
34. Albrecht, M., Strunk, H.P., Hull, R., and Bonar, J.M. (1993) Dislocation glide in {110} planes in semiconductors with diamond or zinc blende structure. *Appl. Phys. Lett.*, **62**, 2206–2208.
35. Guénolé, J., Brochard, S., and Godet, J. (2011) Unexpected slip mechanism induced by the reduced dimensions in silicon nanostructures : atomistic study. *Acta Mater.*, **59**, 7464–7472.
36. Godet, J., Pizzagalli, L., Brochard, S., and Beauchamp, P. (2004) Theoretical study of dislocation nucleation from simple surface defects in semiconductors. *Phys. Rev. B*, **70**, 054109.